Influence of RGO/TiO$_2$ nanocomposite on photo-degrading Rhodamine B and Rose Bengal dye pollutants

A ROSY and G KALPANA* [ORCID]

Department of Physics, Anna University, Chennai 600 025, India
*Author for correspondence (g_kalpa@yahoo.com)

Abstract. Reduced graphene oxide/titanium oxide-nanostructured composite (RGO/TiO$_2$) was prepared by combining Hummer's synthesized graphene oxide and solvothermally synthesized TiO$_2$ nanoparticles (TiO$_2$) through a facile ultrasonication-mediated mechanical mixing method. Structural and morphological evidences from XRD and SEM results confirmed that the as-prepared TiO$_2$ composed of mixed phases, anatase phase with body centred tetragonal crystal structured prism-like architecture, rutile phase with primitive tetragonal crystal-structured bipyramid-like architecture and hence, RGO/TiO$_2$ system exhibited the similar structural and morphological features. Band gap energy of RGO/TiO$_2$ was reduced from 2.98 to 2.91 eV due to the presence of RGO and hence, the light absorption range was extended to visible region. In addition, RGO acted as the electron acceptor and hence, the separation efficiency of photo-generated electron–hole pairs increased effectively, and this prevented the recombination process in RGO/TiO$_2$ system. Thus, RGO/TiO$_2$ system exhibited greater efficiency towards degrading Rhodamine B (RhB) and Rose Bengal (RB) dye pollutants than bare TiO$_2$ under sonophotocatalytic condition with natural sunlight irradiation. The possible mechanisms responsible for the enhanced efficiency are explained in this study using appropriate characterization techniques.

Keywords. Ultrasonication; RGO/mixed phases TiO$_2$; sonophotocatalytic treatment; sunlight irradiation; RhB and RB dye degradation.

1. Introduction

Enormous amount of natural and synthetic dyes are utilized by various industries to add/change colour of substances. Worldwide around 7×10^5 ton of synthetic dyes are produced per year and utilized by various industries such as printing ink, pharmaceutical, food, cosmetics, plastics, photographic, painting, paper industries, etc. Improper disposal of these dye effluents from various industries badly affects our environment and the food chain. Almost all dyes utilized by the industries are carcinogenic, mutagenic and toxic to all living beings.

These toxic dye effluents can be detoxified using photocatalyst in an efficient, cost-effective and non-destructive manner. Titanium oxide (TiO$_2$) is one of the wide band gap semiconductor photocatalysts investigated widely, due to its advantages such as water insolubility, non-toxicity, good chemical stability and high photo-corrosion resistivity [1–3]. TiO$_2$ is found to exist in three different phases, namely anatase, rutile and brookite. Among the three phases, anatase phase TiO$_2$ is known to exhibit a better photocatalytic activity [4,5]. Still, due to its wide band gap (anatase 3.2 eV and rutile 3.0 eV), photoaccelerated electron–hole pairs easily recombine under UV light irradiation and hence, reduces its efficiency [6–9].

Recently, it was reported that [10] dual phases TiO$_2$ (anatase and rutile) provided an efficient pathway for the photo-activated electrons compared to single-phase anatase TiO$_2$. Also, a similar enhancement was achieved in TiO$_2$ (P25 from Degussa) and this enhancement was mainly ascribed to the coexistence of mixed phases (anatase 80% and rutile 20%) in it [11]. Photo-degradation of Orange G (OG) and Yellow 28 (Y28) pollutants using hetero-structure phases (anatase and rutile) TiO$_2$ was investigated, in which the rutile phase extended the range of absorption light wavelength for better activity and also provided a good charge-separation efficiency for photo-activated electron–hole pairs [12]. A complete conversion of bisphenol A pollutant was reported using mixed phases (anatase 43%, rutile 24% and brookite 33%) TiO$_2$ nanocomposite as a photocatalyst and the achieved efficiency was 94% [13]. To further amplify photo-degradation performance in mixed phases of TiO$_2$ for commercial purpose in industries, various approaches were used by the researchers such as doping, composite formation, non-metal loading, etc.

Recently, hybrid materials (combining organic with inorganic materials) have attracted much attention by the researchers to meet commercial needs effectively. It was reported that the efficiency of dual phases TiO$_2$ (anatase 88% and rutile 12%) in degrading formic acid was found to be 58%, which amplified to 66% when supported with graphene oxide (GO) [14]. Mixed phases TiO$_2$ nanofibres wrapped with reduced graphene oxide (rGO) nanocomposite showed almost a complete destruction of methyl orange (MO) pollutant with 99.2% efficiency [15]. Functionalized TiO$_2$
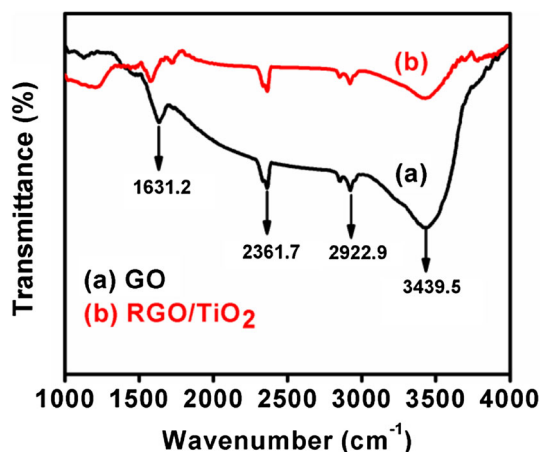
Figure 1. FTIR spectra of (**a**) GO and (**b**) RGO/TiO$_2$.

using organic ligand 2-naphthol exhibited 100% efficiency towards reducing Cr(VI) under sunlight irradiation, which was seven times greater than the bare TiO$_2$ [16]. AgI/meso-TiO$_2$ supported by rGO, exhibited effective visible light degradation towards Rhodamine B (RhB) and MO pollutants [17]. Catechol/TiO$_2$ carbonaceous polymer photocatalyst performed 100% efficiency within 20 min against Cr(VI) reduction under visible-light irradiation [18]. In these photocatalysts, synergistic interactions between the organic and the inorganic materials reduced the optical band gap of TiO$_2$ and extended its light absorption range from UV to visible region. Also, organic materials acted as the electron acceptors and hence, the recombination process was prevented, which resulted in obvious enhancement of TiO$_2$ performance in photocatalytic dye degradation process.

It is an obvious fact that different precursors with different preparation methods can lead to a material with different properties and hence, in the present work, a facile and different technique (ultrasonication-assisted mechanical mixing method) was adapted to prepare RGO/TiO$_2$. Besides, the dye solutions loaded with photocatalysts were subjected to sonication treatment for 30 min before exposing them to sunlight irradiation. This provided better interactions between the photocatalyst and the dye molecules by preventing agglomeration of nanoparticles to retain its high surface area. Thus, both TiO$_2$ and RGO/TiO$_2$ showed reasonable degradation efficiency, however, RGO/TiO$_2$ system showed greater dye-degradation efficiency than TiO$_2$ and the possible mechanisms responsible for the enhancement are explained in this paper.

2. Experimental

2.1 *Synthesis of GO: Hummer's method*

2.1a *Addition of precursors*: Two grams graphite powder (50 μm, 99.5%), 2 g sodium nitrate and 12 g potassium permanganate were added to the volume of 500 ml concentrated sulfuric acid (98%) and mixed thoroughly to obtain homogeneous solution. Temperature of the solution was maintained at 4°C with constant stirring throughout the process.

2.1b *Neutralization process*: Water was added gradually until colour of the solution turns to chocolate-brown. During this process, temperature of the solution was maintained at 4°C. Then, the ice bath was replaced by silicon oil bath and the temperature was gradually raised to 98°C.

2.1c *Addition of hydrogen peroxide and water*: Sixteen millilitres of hydrogen peroxide and 24 ml of water (1:1.5 ratio) solution was prepared freshly and slowly added to the
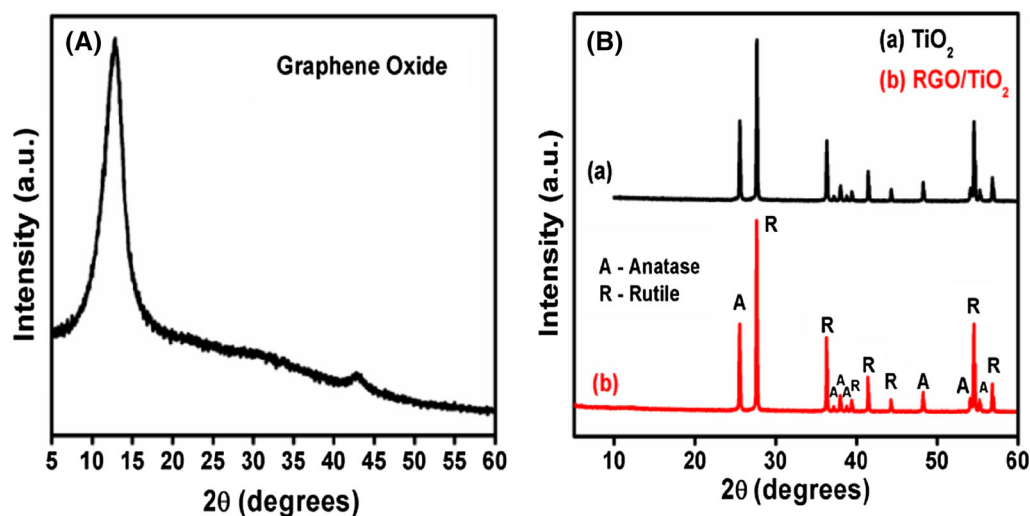

Figure 2. XRD patterns of (**A**) GO and (**B**) (a) TiO$_2$ and (b) RGO/TiO$_2$.
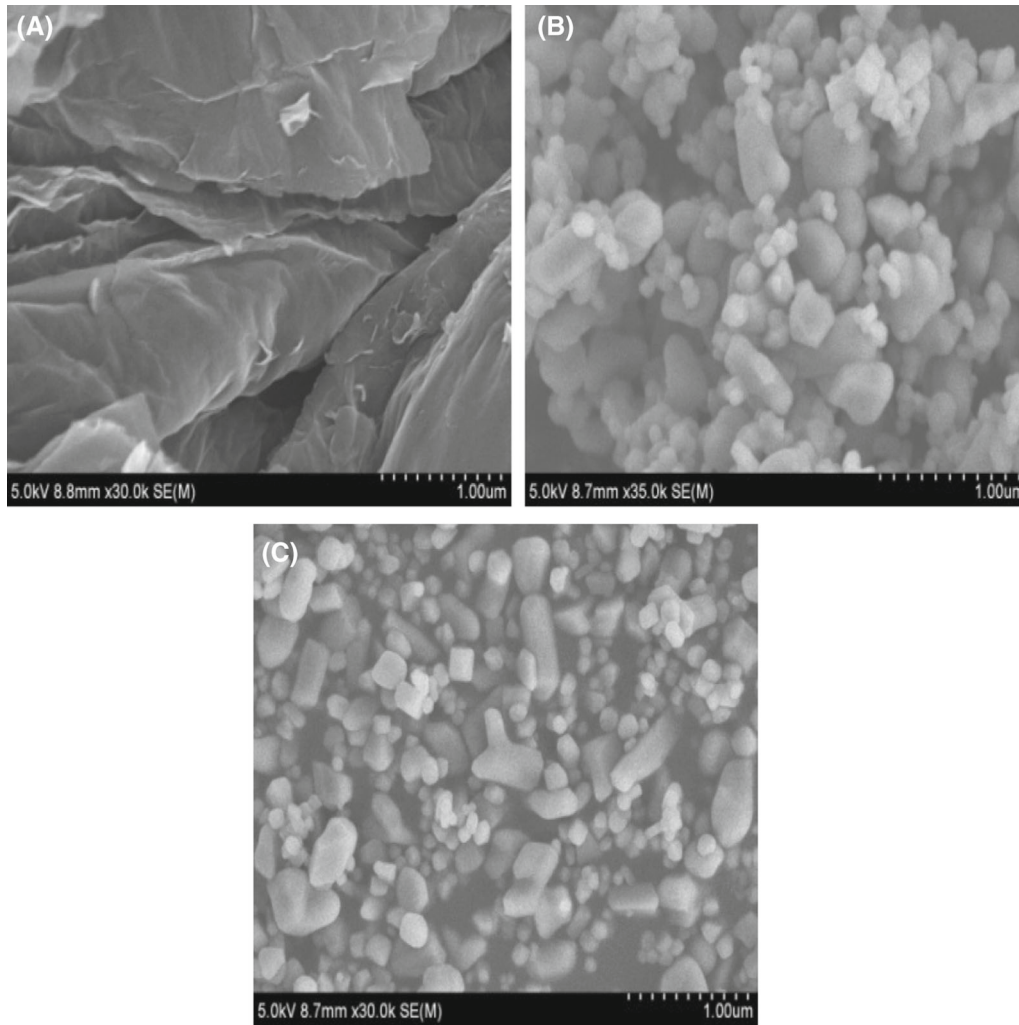
Figure 3. SEM images of (**a**) GO, (**b**) TiO$_2$ and (**c**) RGO/TiO$_2$.
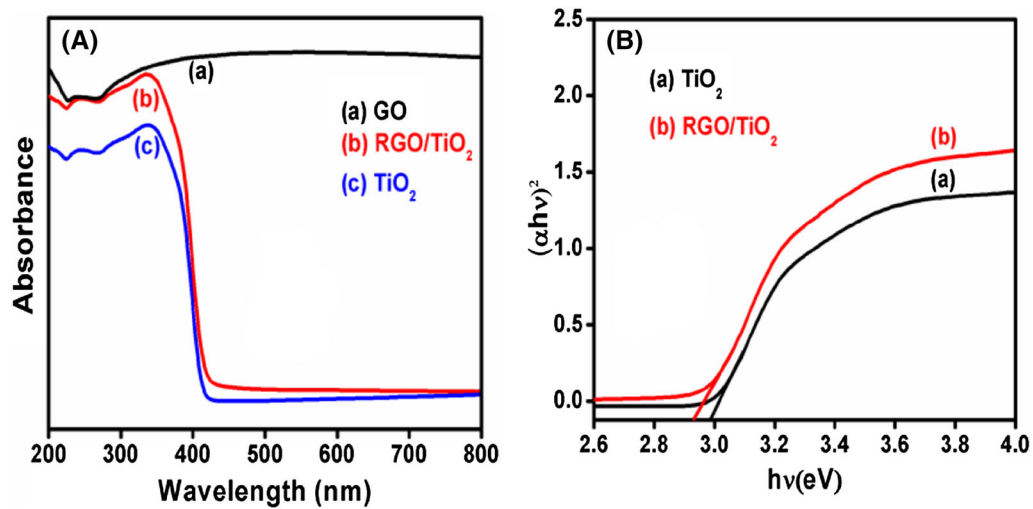
Figure 4. (**A**) UV–diffuse reflectance spectra and (**B**) Tauc plot.
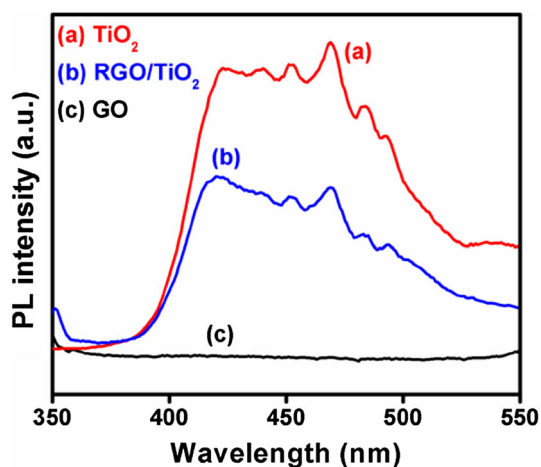
Figure 5. PL spectrum of (**a**) TiO_2, (**b**) RGO/TiO_2 and (**c**) GO.

previous solution. After complete addition, 600 ml volume of water was added to the solution.

2.1d *Addition of HCl*: The water was poured away completely without disturbing the settled GO at the bottom. Thereafter, 16 ml of concentrated HCl (37%) was added with constant stirring and the solution was diluted with 1000 ml water.

2.1e *Washing and sonication*: Water was poured away completely without disturbing the settled GO at the bottom of the container. The obtained product was filtered, centrifuged and washed thoroughly with plenty of water till the pH of the solution becomes neutral. Then, the solution was sonicated for few hours and then dried at 200°C in an oven to obtain high-quality GO.

2.2 *Synthesis of mixed phases TiO₂ nanoparticles: solvothermal method*

Titanium(IV) iso-propoxide (Alfa Aesar, 95%, $C_{12}H_{28}O_4Ti$, 284.22 g mol^{-1}) was added to ethanol–water solution with ratio of titanium(IV) iso-propoxide:ethanol:water::1:3:8 as mentioned in the literature [19] and the solution was stirred for few hours at 70°C. Then, the solution was solvothermally treated using Teflon-lined stainless steel autoclave at 120°C for 24 h. The obtained solution was sonicated, centrifuged and then dried in an oven. Finally, calcined at 700°C for 5 h to obtain high-purity mixed phases TiO_2 nanoparticles.

2.3 *Preparation of RGO/TiO₂-nanostructured composite*

Eight milligrams of as-synthesized GO and 1 g of TiO_2 nanoparticles were dissolved in a volume of 50 ml distilled water. Thereafter, the solution was sonicated in acid medium for 1 h, centrifuged and then dried in an oven

at 100°C to obtain high-purity RGO/TiO_2-nanostructured composite.

2.4 *Sonophotocatalytic experiment*

For dye-degradation experiment, each 0.1 g of TiO_2 and RGO/TiO_2 were suspended separately in two different RhB (0.04 mg RhB in 100 ml of water) and Rose Bengal (RB) (0.02 mg RB in 100 ml of water) dye solutions. The above solutions were sonicated for 30 min and then, magnetically stirred for 30 min to obtain adsorption–desorption equilibrium of dye on catalyst before exposing the dye solutions under sunlight irradiation and hence, this process was mentioned as sonophotocatalytic condition in the present work. Thereafter, the solutions were exposed to sunlight and withdrawn (about 3 ml) at different time intervals, centrifuged to measure the concentration of the dye solutions through UV–visible absorption spectrophotometer. The experiment was performed under the following conditions: tropical climate (geographical location: Chennai; 13.04°N and 80.17°E on the southern-east coast of India, average temperature: 39°C) and the average sunlight intensity of 1.2×10^5 lx (measured using LT-Lutron LX-10/A digital Lux meter (TES Electronic Corp., Taiwan).

3. Results and discussion

3.1 *Investigation of functional groups: FTIR analysis*

Figure 1 shows FTIR spectra of (a) GO and (b) RGO/TiO_2. From the result, it was concluded that 1631.2, 2361.7, 2922.9 and 3439.5 cm^{-1} were corresponding to sp^2 hybridized C=C in-plane vibrations, CO_2, C–H and C–OH vibrations, respectively [20]. However, from 1600 to 1850 cm^{-1} corresponding to C=O peaks were not that sharp in as-prepared GO and RGO/TiO_2, which confirmed the reduction of GO into RGO. For TiO_2 sample, the wavenumber ranges from 400 to 800 cm^{-1}, which usually represent stretching vibration of Ti–O–Ti [21], and this is not shown in figure 1, since here, the covered range was from 1000 to 4000 cm^{-1}.

3.2 *Structural investigation: XRD analysis*

Figure 2A shows powder XRD pattern of GO, a predominant peak position at 12.8° (2θ) confirmed the phase formation of GO with 0.69 nm *d* spacing calculated from Bragg's formula, $2d \sin \theta = n\lambda$, the similar result was observed by Radka Pocklanova *et al* [22]. In figure 1B, (a) and (b) represent powder XRD patterns of TiO_2 and RGO/TiO_2, respectively, and from the results, it was confirmed that the as-prepared TiO_2 nanoparticles composed of mixed phases (anatase 27% and rutile 73%) and their proportions were calculated using the following equation (1) [23].

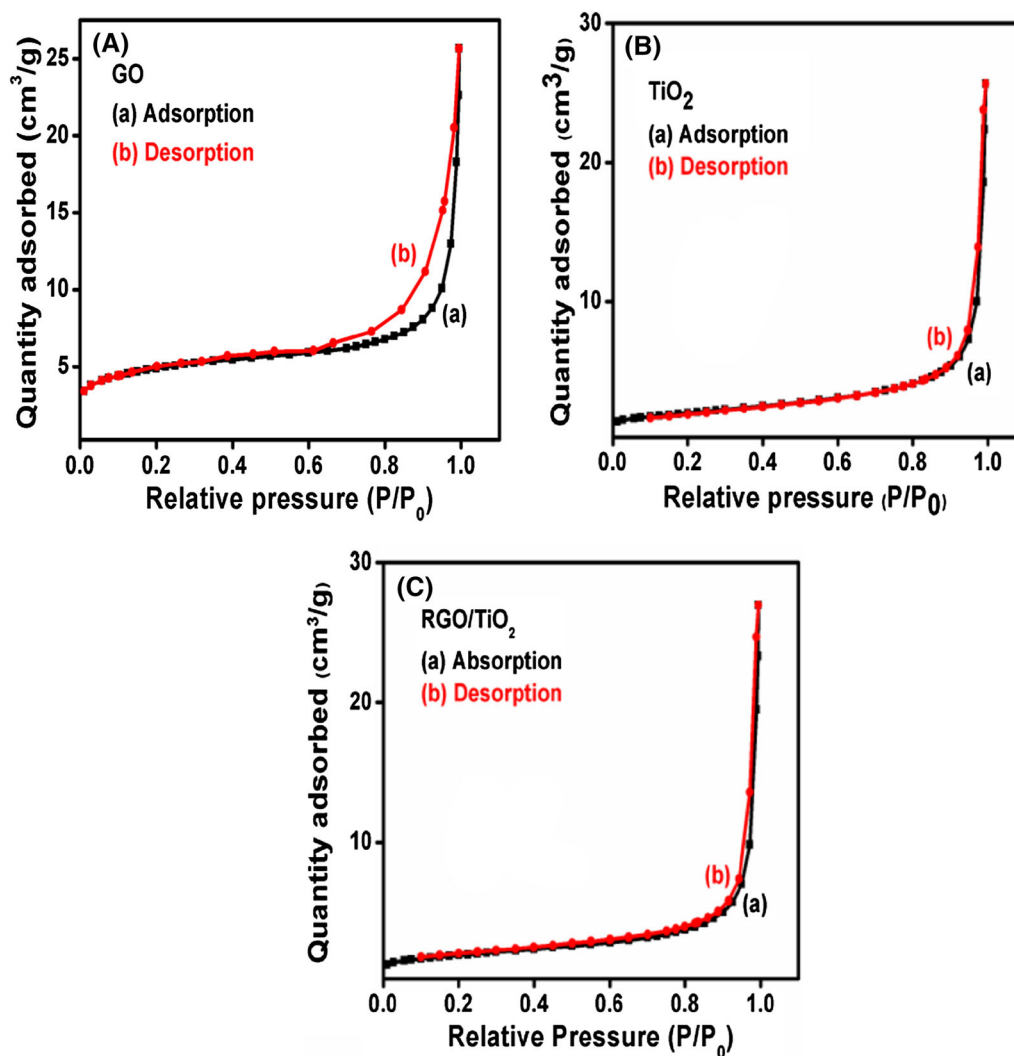$$\text{Anatase}(\%) = 100/\{1 + [1.265(I_{\text{max rutile}}/I_{\text{max anatase}})]\} \quad (1)$$

Figure 6. Adsorption–desorption isotherms of (**A**) GO, (**B**) TiO$_2$ and (**C**) RGO/TiO$_2$.

Table 1. Summarization of crystallite size (D), band gap (E_g), surface area (SA), pore size (PS), pore volume (PV), RhB dye-degradation efficiency (RhB%) and RB dye-degradation efficiency (RB%).

Samples	D (nm)	E_g (eV)	SA (m^2 g^{-1})	PS (nm)	PV (cm^3 g^{-1})	RhB%	RB%
GO	—	—	163	9.74	0.042	—	—
TiO$_2$	69	2.98	66	25.148	0.0397	75.5	75
RGO/TiO$_2$	64	2.91	68	23.283	0.040	98	94

Anatase TiO$_2$ peaks were well-indexed with standard JCPDS card no. 21-1272, body-centred tetragonal crystal system with a space group $I4_1/amd$, while the rutile peaks were well indexed with standard JCPDS card no. 76-1940, primitive tetragonal crystal system with a space group $P4_2/mnm$.

$$D = K\lambda/\beta\cos\theta \qquad (2)$$

Using the Scherrer equation (2), the calculated average crystallite sizes (D) for TiO$_2$ and RGO/TiO$_2$ using the plane (110) were 69 and 64 nm, respectively.

3.3 Morphological features: SEM analysis

Figure 3a, b and c represents the surface topography of GO, TiO$_2$ and RGO/TiO$_2$, imaged at an operating voltage of 5 kV, respectively. GO showed exfoliated flakes with wavy wrinkles architecture and the individual GO sheets were closely connected with each other with a leaf-like architecture, which confirmed the two-dimensional network of GO, which was in good agreement with already reported result by He *et al* [24] and Gurunathan *et al* [25]. The as-prepared TiO$_2$
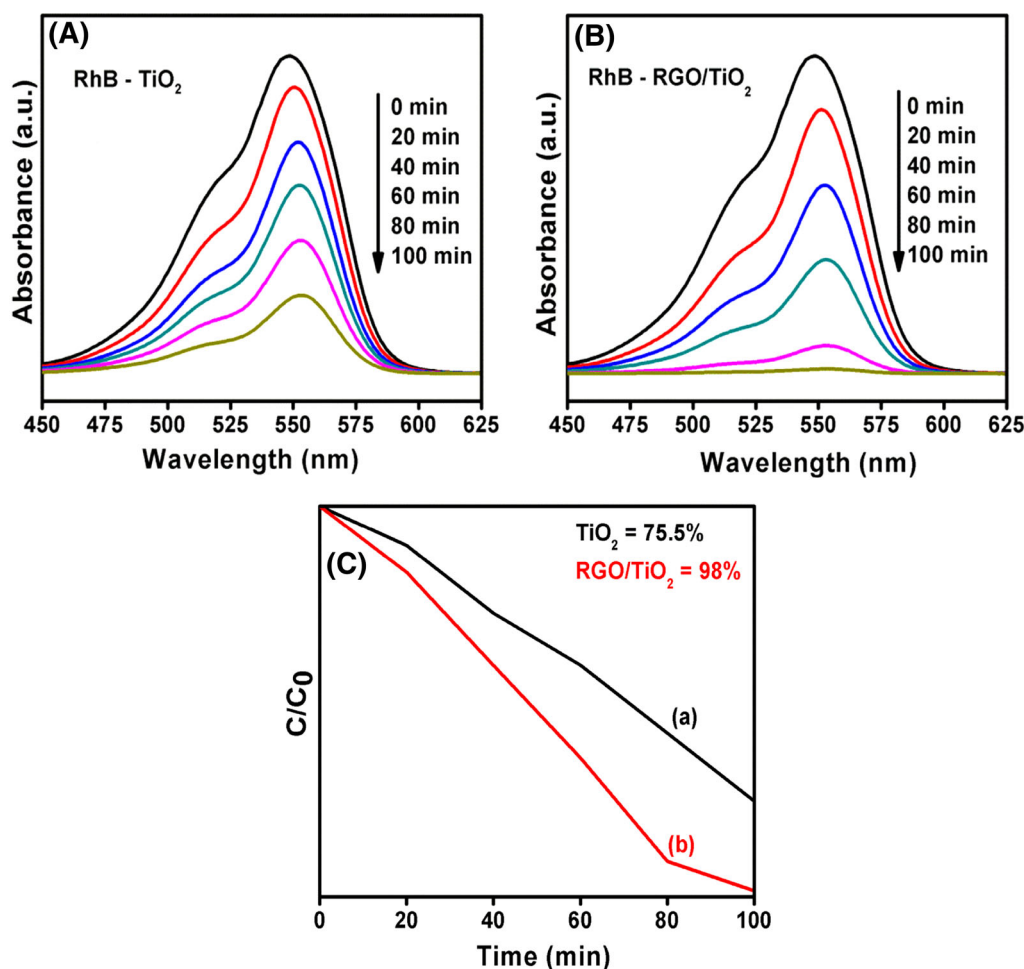
Figure 7. UV–visible spectrum displaying the photocatalytic degradation measurements of RhB dye by photocatalysts: (**A**) TiO_2, (**B**) RGO/TiO_2 and (**C**) concentration *vs*. time plot.

nanoparticles contained tetragonal bipyramid-like architecture for anatase phase and tetragonal prism-like architecture for rutile phase with little aggregated particles. The similar surface morphological features for anatase and rutile phases with well-separated particles were reported by Teruhisa Ohno [26]. RGO/TiO_2 system exhibited the similar morphological features of anatase and rutile with well-separated particles and hence, the system exhibited smaller crystallite size than bare TiO_2, well-supported with XRD result (RGO suppressed the aggregation effect of nanoparticles).

3.4 *Optical properties: UV–DRS analysis*

Figure 4a shows diffuse reflectance spectra (DRS) of as-prepared GO, RGO/TiO_2 and TiO_2 materials recorded in the range of 200–800 nm, respectively. The red shift observed for RGO/TiO_2 was attributed to synergistic and intermolecular interactions between RGO and TiO_2. Besides, the as-prepared TiO_2 showed smaller band gap than the reported values, for anatase 3.2 eV and for rutile 3.0 eV [27]. This could be due to the flat band potential (E_{FB}) difference between anatase

(-0.45 eV) and rutile phases (-0.37 eV) and also due to the dominant rutile phase, because the rutile phase TiO_2 (2.98 eV) generally exhibits smaller band gap than anatase phase TiO_2 (3.05 eV) [28]. Figure 3b shows Tauc plot of as-prepared TiO_2 and RGO/TiO_2, from which the band gap values were calculated. Influence of RGO in TiO_2 lattice enhanced the electron transfer mechanism from anatase TiO_2 to rutile TiO_2 and to RGO through newly created intermediate energy levels just below the conduction band of TiO_2. Hence, the band gap of RGO/TiO_2 was reduced from 2.98 to 2.91 eV. This unique band gap features of RGO/TiO_2 system played a crucial role in degrading dyes under sonophotocatalytic condition with natural sunlight irradiation than its individual counterpart.

3.5 *Optical properties: PL spectra*

Figure 5a, b and c represents the photoluminescence (PL) emission spectra of as-prepared TiO_2, RGO/TiO_2 and GO materials recorded at a wavelength range from 350 to 550 nm with an excitation wavelength of 325 nm. RGO/TiO_2 exhibited lower emission intensity than RGO-free TiO_2, which
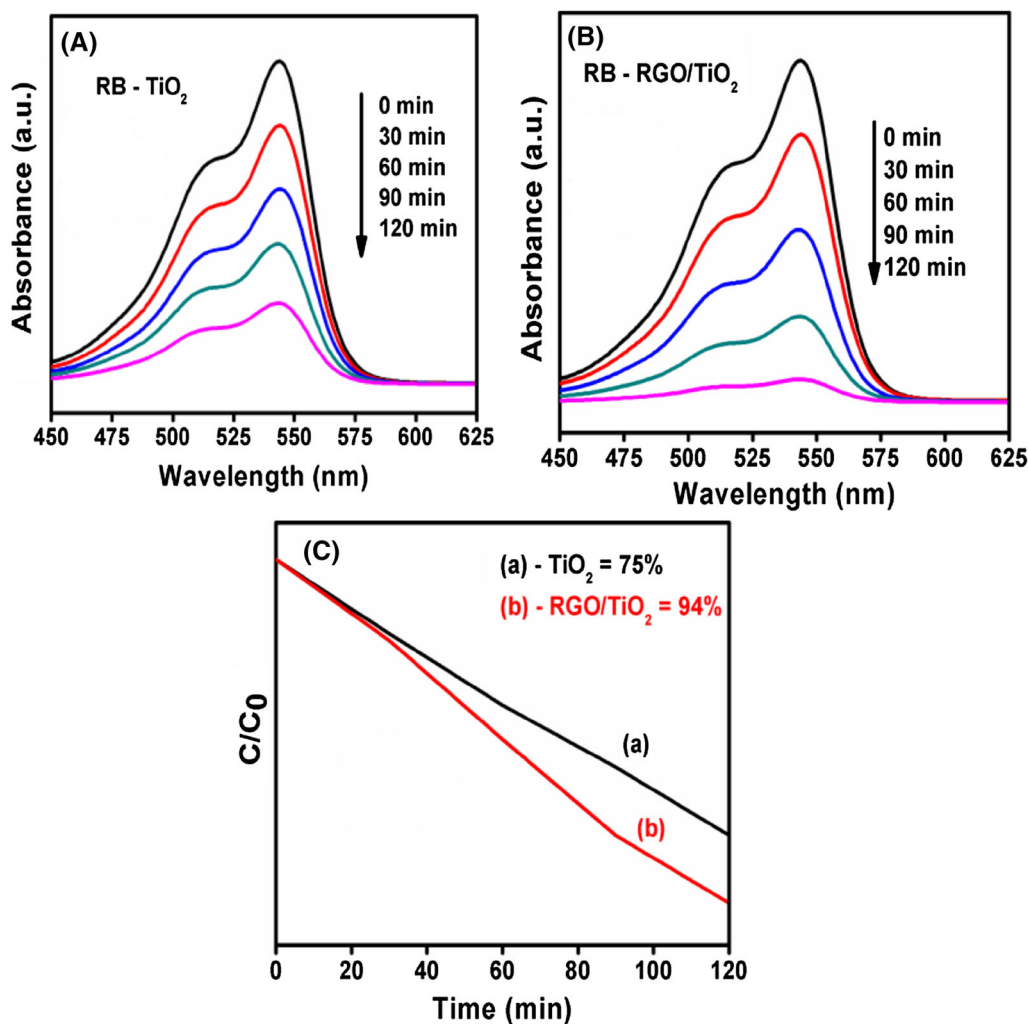
Figure 8. UV–visible spectrum displaying the photocatalytic degradation measurements of RB dye by photocatalysts: (**A**) TiO_2, (**B**) RGO/TiO_2 and (**C**) concentration *vs*. time plot.

could be attributed to the rapid migration of electrons from the conduction band of anatase TiO_2 to conduction band of rutile TiO_2 and to RGO. This rapid migration of electrons and holes in RGO/TiO_2 heterostructure leads to suppress the recombination rate of photo-excited electron–hole pairs, due to which the composite system exhibited lower PL emission intensity than its individual counterparts (well-supported with DRS result). Hence, the excited electrons in the dye solution combined with oxygen to form photo-excited superoxide (O_2^-*) radicals, which were the main reactive species to react with dye pollutants effectively and enhanced the photocatalytic dye-degradation efficiency of RGO/TiO_2.

3.6 *Surface area and pore size measurements: BET analysis*

Figure 6a, b and c represents adsorption–desorption isotherms of GO, TiO_2 and RGO/TiO_2 measured at relative pressure range from 0 to 1, respectively, and all the three samples exhibited typical type IV IUPAC classification. Their surface area, pore size and pore volume distributions are summarized in table 1. In addition, their pore size distribution also implies that all the three samples contained mesoporous structures. However, the mesoporous hysteresis loop could be observed in GO and not in TiO_2 and RGO/TiO_2, and also, adsorption–desorption isotherms increased rapidly at relative pressure closer to one which resembles type II isotherm curves, this reveals that the as-prepared samples also contained large macropores within them. Specific surface area of RGO/TiO_2 was increased from 66 to 68 $m^2 \ g^{-1}$ due to the smaller crystallite size and well-separated particles (good agreement with XRD and SEM results). Also the increased surface area could be due to the influence of RGO ($< 2 \ g \ cm^{-3}$), which has very low density than TiO_2 (4.038 $g \ cm^{-3}$) and hence, the composite system exhibited increased surface area than bare TiO_2.

3.7 *Investigation of photocatalytic dye-degradation efficiency*

Efficiency of TiO_2 and RGO/TiO_2 was investigated in degrading RhB and RB dye pollutants under natural sunlight irradiation with sonophotocatalytic condition. Sunlight-exposed dye solutions were collected for UV–visible absorption spectrum analysis at different time intervals and are displayed in figures 7 and 8, from the spectra, their efficiency was calculated using the following equation (3):

$$\text{Efficiency}(\%) = \{1 - (C/C_0)\} \times 100, \tag{3}$$

where C_0 is the initial concentration of the dye solution and C the final concentration of the dye solution. In degrading RhB dye pollutant, TiO_2 and RGO/TiO_2 were found to exhibit 75.5 and 98% efficiencies in degrading RB dye pollutant, their efficiencies were found to be 75 and 94%, respectively. Both TiO_2 and RGO/TiO_2 exhibited reasonable efficiencies, which were mainly ascribed to the sonophotocatalytic treatment, because this special condition retained the crystalline phase, high surface area and prevented the aggregation of particles. However, a greater efficiency was achieved in RGO/TiO_2, which was attributed to the improved features of RGO/TiO_2 than RGO-free TiO_2 as follows: (i) synergistic and intermolecular interactions between RGO and TiO_2 heterostructure, (ii) crystallite size in the nano-regime, (iii) mixed phases with special morphological architectures, (iv) significant specific-surface area and (v) good separation of photo-excited electron–hole pairs.

4. Conclusion

RGO/mixed phases (anatase and rutile) TiO_2-nanostructured composite was successfully prepared by a facile ultrasonication-assisted mechanical mixing technique. Structure and morphological features from XRD and SEM results confirmed the successful formation of RGO/TiO_2. The composite system exhibited improved features than RGO-free TiO_2 for effective degradation of dye pollutants under sonophotocatalytic condition with natural sunlight irradiation. In degrading both RhB and RB dye pollutants, RGO/TiO_2 exhibited more than 90% efficiency and hence, this photocatalyst can be an effective, sunlight-driven and economical catalyst in industrial applications for treating toxic dye effluents.

References

[1] Hoffmann M R 1995 *Chem. Rev.* **95** 69
[2] Fukahori S 2003 *Environ. Sci. Tech.* **37** 1048
[3] Antonopoulou M 2013 *Clean Soil Air Water* **41** 593
[4] Sclafani A 1996 *J. Phys. Chem.* **100** 13655
[5] Jung H S 2009 *Electron Mater. Lett.* **5** 73
[6] Kowalska E 2008 *J. Phys. Chem. C* **112** 1124
[7] Dozzi M 2013 *J. Photochem. Photobiol. C: Photochem. Rev.* **14** 13
[8] Chen C C 2010 *Chem. Soc. Rev.* **39** 4206
[9] Chen X 2010 *Chem. Rev.* **110** 6503
[10] Mi Y 2015 *Sci. Rep.* **5** 11482
[11] Hurum D C 2003 *J. Phys. Chem. B* **107** 4545
[12] Kordouli E 2015 *J. Catal. Today* **252** 128
[13] Kaplan R 2016 *J. Appl. Catal. B: Environ.* **18** 465
[14] Hamandi M 2017 *J. Mol. Catal.* **432** 125
[15] Lavanya T 2017 *J. Environ. Chem. Eng.* **5** 494
[16] Karthik P 2015 *RSC Adv.* **5** 39752
[17] Vinoth R 2016 *Phys. Chem. Phys.* **18** 5179
[18] Karthik P 2017 *J. Mater. Chem. A* **5** 384
[19] Obregon S 2016 *Mater. Lett.* **173** 174
[20] Sudesh B 2013 *Supercond. Sci. Technol.* **26** 095008
[21] Othman S H 2012 *J. Nanomater.* **2012** ID 718214
[22] Pocklanova R 2016 *Mol. Catal. A: Chem.* **424** 121
[23] Rajesh J 2007 *Sci. Technol. Adv. Mater.* **8** 455
[24] He H 2010 *J. Chem. Mater.* **22** 5054
[25] Gurunathan S 2014 *Int. J. Nano Med.* **9** 363
[26] Ohno T 2002 *New J. Chem.* **26** 1167
[27] Shokri A 2016 *J. Environ. Chem. Eng.* **45** 85
[28] Di Paola A 2013 *Catalysts* **3** 36